General Synthesis of Mesoporous Spheres of Metal Oxides and Phosphates

Angang Dong, Nan Ren, Yi Tang,* Yajun Wang, Yahong Zhang, Weiming Hua, and Zi Gao

Shanghai Key Laboratory of Molecular Catalysis and Innovative Materials, Department of Chemistry, Fudan University, Shanghai 200433, P. R. China

Received December 30, 2002; E-mail: ytang@fudan.ac.cn

Mesoporous materials with variable compositions, controllable morphologies, and tunable wall structures are of particular interest for catalysis, adsorption, and applications as hosts for nanomaterials synthesis.[1−9] Recently, the preparation of spherical mesoporous particles in the micrometer- and submicrometer-size range has received much attention because of their broad applications in chromatography, bioseparation, and nanotechnology.[4−8] On the basis of a modified Stöber reaction process, monodisperse mesoporous SiO_2 spheres with tunable particle size have been synthesized by Unger's group.[4a] However, up to now, there are still no general methods to prepare mesoporous spheres built of nonsiliceous inorganic materials.[5−8]

Recently, ordered mesoporous carbon, which is an inverse replica templated from mesoporous silica by a nanocasting route,[9] has attracted increasing attention, due to its potential applications as catalyst supports, adsorbents, and other advanced materials.[9b] More recently, mesoporous carbon such as CMK-3[9c] has been successfully employed as further template to achieve the reversible replication of ordered mesoporous silica.[10] Additionally, some mesoporous oxides have also been templated from activated carbons.[11] These may open a new possibility to synthesize mesoporous materials for the rigid framework of carbon templates different from the commonly used surfactant templates.[1−5]

Here, we present a versatile procedure based on the two-step nanocasting route to prepare monodisperse and high-surface-area mesoporous spheres of tailored compositions, as well as controllable crystalline phases and defined morphologies. To begin, uniform mesoporous silica spheres prepared by Unger's method[4a] were used as the template for the formation of mesoporous carbon spheres by the nanocasting technique.[9a] Mesoporous inorganic spheres were then obtained by templating the specific precursor with carbon spheres. Typically, the pore system of carbon template was infiltrated with the desired precursor such as alkoxides or inorganic salts (dissolved in organic solvent) by wet impregnation. After removing the redundant precursor by centrifugation, the hydrolysis of precursor was initiated by exposure to the moisture in air. The mesoporous inorganic spheres were finally obtained by crystallization or polymerization of inorganic species at 600 °C (or 950 °C for rutile-type titania formation) in nitrogen for 6 h, coupled with removal of carbon at 550 °C in air for 8 h. The carbon content after calcination was ca. 0.7%, determined by elemental analysis.

Because of the excellent structure-directing ability of carbon template resulting from its rigid framework and high chemical stability, various mesoporous spheres including single- and multi-component metal oxides and phosphates can be easily prepared by choosing appropriate precursors, as we have done here (Table 1). Another important feature of carbon is its high thermal stability in inert atmosphere; therefore, not only can inorganic species be highly crystallized or polymerized but their crystalline phases may also be tailored by controlling crystallization temperatures. In addition, it is interesting to find that either solid or hollow spheres can be

Table 1. Precursors and Properties of the Representative Mesoporous Inorganic Spheres

sample[a]	precursor[b]	wall structure (by XRD)	S_{BET} (m^2/g)	w^d (nm)	V^e (cm^3/g)
TiO_2	TIP	anatase	158	6	0.30
TiO_2	TIP	anatase/rutile	143	7	0.34
ZrO_2	$ZrCl_4$	T/M^c	96	6	0.14
Al_2O_3	$Al(O^sBu)_3$	γ-Al_2O_3	442	4	0.61
$Ti_2Si_3O_y$	TIP/APS	amorphous	455	4	0.33
Ti_2ZrO_y	TIP/ $ZrCl_4$	amorphous	117	4	0.14
ZrP	$ZrCl_4$/TEP	amorphous	228	5	0.32
AlP	$AlCl_3$/TEP	amorphous	474	5	0.60

^{a} ZrP and AlP are zirconium phosphate and aluminum phosphate, respectively. ^{b} TIP, APS, and TEP are titanium isopropoxide, (3-amino-propyl)triethoxysilane, and triethylphosphate, respectively. ^{c} T and M are the tetragonal and monoclinic phases of solid mesoporous ZrO_2 spheres, respectively. ^{d} w is the pore size calculated from nitrogen data based on the BJH model of the desorption branch. ^{e} V is the pore volume.
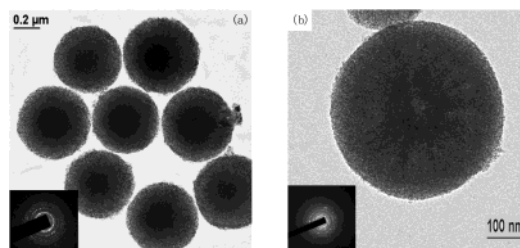

Figure 1. TEM images and ED patterns (inset) of mesoporous anatase-type (a) and anatase/rutile-type (b) TiO_2 spheres.

produced in some cases by changing the polarity of the precursor to match the hydrophobic character of carbon.

The transmission electron microscopy (TEM) image of mesoporous anatase-type TiO_2 spheres (Figure 1a) prepared from titanium isopropoxide shows that the discrete and uniform spherical morphology and the disordered pore structure of the original SiO_2 spheres[4a] are well preserved in the final product after two steps of replication. The TiO_2 sphere size (500−600 nm) is somewhat smaller than that of carbon spheres (800−900 nm), resulting from the shrinkage after the removal of carbon. The electron diffraction (ED) pattern (Figure 1a, inset) verifies that the pore walls of TiO_2 spheres are composed of crystalline anatase, which is further confirmed by X-ray diffraction (XRD) analysis. The size of anatase nanocrystals is determined as 10 nm by TEM at high magnification. If the crystalline temperature of titania was increased to 950 °C in nitrogen, mesoporous anatase/rutile bicrystalline TiO_2 spheres (Figure 1b) were generated after the removal of carbon. The weight fraction of rutile phase calculated from the XRD integrated intensities of rutile (110) and anatase (101) peaks[12] is 60%. The shape of the N_2 adsorption/desorption isotherms of both anatase- and anatase/rutile-type TiO_2 spheres present the characters of their mesoporosity, and the Brunauer−Emmett−Teller (BET) surface areas are both at about 150 m^2/g.
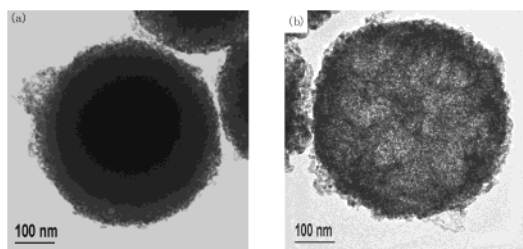
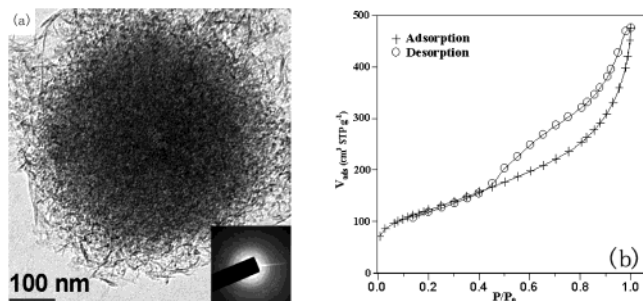**Figure 2.** TEM images of solid (a) and hollow (b) mesoporous ZrO_2 spheres.

Figure 3. (a) TEM image and ED pattern (inset) and (b) N_2 adsorption/desorption isotherms of mesoporous γ-Al_2O_3 spheres.

The polarity of the precursor had a great effect on the final product morphologies due to the hydrophobic nature of carbon template. For example, in the preparation of mesoporous ZrO_2 spheres, when $ZrCl_4$ was dissolved in a mixture of ethanol and cyclohexane (1:1, v/v) as the initial precursor, the resulting ZrO_2 spheres exhibited a solid structure (Figure 2a) similar to that of TiO_2 spheres, whereas using the ethanol solution of $ZrCl_4$ as precursor, only hollow mesoporous ZrO_2 spheres (Figure 2b) were obtained. This result indicated that it was difficult to infiltrate the inner parts of the carbon spheres with the ethanol solution of $ZrCl_4$, which was somewhat hydrophilic, resulting in hollow ZrO_2 spheres after calcination. On the contrary, the precursor became very hydrophobic with the addition of cyclohexane and therefore could fill all the parts of carbon template to lead to solid ZrO_2 spheres.

Different from TiO_2 and ZrO_2 spheres which are both composed of particulate nanocrystals, mesoporous Al_2O_3 spheres (Figure 3a) prepared from aluminum *sec*-butoxide are composed of interesting lath-shaped nanoparticles. The XRD pattern exhibits reflections consistent with γ-Al_2O_3. A similar phenomenon was also found by Zhang et al.[2b] in the preparation of mesoporous MSU-γ Al_2O_3 by hydrolysis of aluminum salts in the presence of nonionic surfactant. The N_2 adsorption/desorption isotherms in Figure 3b indicate the mesoporosity of γ-Al_2O_3 spheres, although their pore size distribution is broader than that of TiO_2 spheres, probably due to their special nanoparticle morphology. The BET surface area of γ-Al_2O_3 spheres is 442 m^2/g, much larger than the reported data of both conventional γ-Al_2O_3 (185−250 m^2/g) and MSU-γ Al_2O_3 (299−370 m^2/g).[2b]

In addition to single-component, this two-step procedure can be readily extendible to multicomponent mesoporous oxides and metal phosphates using the homogeneously mixed precursors (Table 1). The obtained mesoporous spheres of mixed oxides are generally amorphous, indicating that the two components are distributed uniformly in the wall.[2a] Figure 4a shows the TEM image of mesoporous zirconium phosphate (ZrP) spheres prepared using triethyl phosphate and $ZrCl_4$ as phosphorus source and zirconium
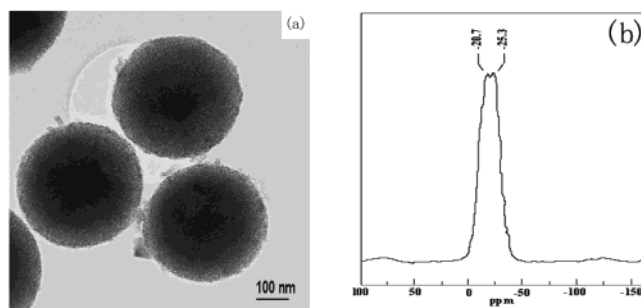

Figure 4. TEM image (a) and ^{31}P NMR spectrum (b) of mesoporous zirconium phosphate spheres.

source, respectively. The ^{31}P NMR spectrum of mesoporous ZrP spheres in Figure 4b shows two peaks at −20.7 and −25.2 ppm, corresponding to tetrahedral phosphorus of connectivity 3 and 4 [$P(OZr)_3OH$ and $P(OZr)_4$], respectively. This result is in agreement with the previously reported data of mesoporous ZrP after calcination.[3a]

In conclusion, we have adopted a two-step nanocasting route to prepare monodisperse mesoporous inorganic spheres with pore walls of variable compositions and controllable crystalline phases. In addition, hollow mesoporous spheres can be obtained in some cases, depending on the polarity of the precursor. These novel mesoporous inorganic spheres are expected to have a variety of applications in chromatography, catalysis, and nanotechnology.

Supporting Information Available: Figure S1, S2, S3, S4, S5, and S6 (PDF). This material is available free of charge via the Internet at http://pubs.acs.org.

References

(1) (a) Kresge, C. T.; Leonowicz, M. E.; Roth, W. J.; Vartuli, J. C.; Beck, J. S. *Nature* **1992**, *359*, 710. (b) Inagaki, S.; Guan, S.; Ohsuna, T.; Terasaki, O. *Nature* **2002**, *416*, 304.
(2) (a) Yang, P.; Zhao, D.; Margolese, D. I.; Chmelka, B. F.; Stucky, G. D. *Nature* **1999**, *396*, 152. (b) Zhang, Z.; Hicks, R. W.; Pauly, T. R.; Pinnavaia, T. J. *J. Am. Chem. Soc.* **2002**, *124*, 1592. (c) Wong, M. S.; Jeng, E. S.; Ying, J. Y. *Nano Lett.* **2002**, *2*, 637.
(3) (a) Jiménez-Jiménez, J.; Maireles-Torres, P.; Olivera-Pastor, P.; Rodríguez-Castellón, E.; Jiménez-López, A.; Jones, D. J.; Rozière, J. *Adv. Mater.* **1998**, *10*, 812. (b) Serre, C.; Auroux, A.; Gervasini, A.; Hervieu, M.; Férey G. *Angew. Chem., Int. Ed.* **2002**, *41*, 1594.
(4) (a) Grun, M.; Buchel, C.; Kumar, D.; Schumacher, K.; Bidlingmaier, B.; Unger, K. K. *Stud. Surf. Sci. Catal.* **2000**, *128*, 155. (b) Lu, Y.; Fan, H.; Stump, A.; Ward, T. L.; Rieker, T.; Brinker, C. J. *Nature* **1999**, *398*, 223. (c) Bibby, A.; Mercier, L. *Chem. Mater.* **2002**, *14*, 1591.
(5) Wang, L.; Tomura, S.; Maeda, M.; Ohashi, F.; Inukai, K.; Suzuki, M. *Chem. Lett.* **2000**, 1414.
(6) Subramanian, A.; Carr, P. W.; McNeff, C. V. *J. Chromatogr., A* **2000**, *890*, 15.
(7) Jiang, Z.; Zuo, Y. *Anal. Chem.* **2001**, *73*, 686.
(8) Meyer, U.; Larsson, A.; Hentze, H.; Caruso, R. A. *Adv. Mater.* **2002**, *12*, 1768.
(9) (a) Ryoo, R.; Joo, S. H.; Jun, S. *J. Phys. Chem. B* **1999**, *103*, 7743. (b) Joo, S. H.; Choi, S. J.; Oh, I.; Kwak, J.; Liu, Z.; Terasaki, O.; Ryoo, R. *Nature* **2001**, *412*, 169. (c) Jun, S.; Joo, S. H.; Ryoo, R.; Kruk, M.; Jaroniec, M.; Liu, Z.; Ohsuna, T.; Terasaki, O. *J. Am. Chem. Soc.* **2000**, *122*, 10712.
(10) (a) Kang, M.; Yi, S. H.; Lee, H. I.; Yie, J. E.; Kim, J. M. *Chem. Commun.* **2002**, 1944. (b) Lu, A.; Schmidt, W.; Taguchi, B.; Spliethoff, B.; Tesche, B.; Schüth, F. *Angew. Chem., Int. Ed.* **2002**, *41*, 3489.
(11) (a) Schwickardi, M.; Johann, T.; Schmidt, W.; Busch, O.; Schuth, F. *Stud. Surf. Sci. Catal.* **2002**, *143*, 93. (b) Wakayama, H.; Itahara, H.; Tatsuda, N.; Inagaki, S.; Fukushima, Y. *Chem. Mater.* **2001**, *13*, 2392.
(12) Zhang, H.; Banfield, J. F. *J. Phys. Chem. B* **2000**, *104*, 3481.

JA029964B